The effects of *Tmc1 Beethoven* mutation on mechanotransducer channel function in cochlear hair cells

Maryline Beurg, Adam C. Goldring, and Robert Fettiplace

Department of Neuroscience, University of Wisconsin School of Medicine and Public Health, Madison, WI 53706

Sound stimuli are converted into electrical signals via gating of mechano-electrical transducer (MT) channels in the hair cell stereociliary bundle. The molecular composition of the MT channel is still not fully established, although transmembrane channel–like protein isoform 1 (TMC1) may be one component. We found that in outer hair cells of Beethoven mice containing a M412K point mutation in TMC1, MT channels had a similar unitary conductance to that of wild-type channels but a reduced selectivity for Ca^{2+}. The Ca^{2+}-dependent adaptation that adjusts the operating range of the channel was also impaired in Beethoven mutants, with reduced shifts in the relationship between MT current and hair bundle displacement for adapting steps or after lowering extracellular Ca^{2+}; these effects may be attributed to the channel's reduced Ca^{2+} permeability. Moreover, the density of stereociliary CaATPase pumps for Ca^{2+} extrusion was decreased in the mutant. The results suggest that a major component of channel adaptation is regulated by changes in intracellular Ca^{2+}. Consistent with this idea, the adaptive shift in the current–displacement relationship when hair bundles were bathed in endolymph-like Ca^{2+} saline was usually abolished by raising the intracellular Ca^{2+} concentration.

INTRODUCTION

Our sense of hearing depends on sound stimuli evoking submicrometer displacements of bundles of stereocilia or hairs that project from the upper surface of the eponymous hair cells (Schwander et al., 2010; Fettiplace and Kim, 2014). Hair bundle motion is then transformed into an electrical signal by activation of mechanically gated ion channels located at the tips of the shorter stereocilia (Beurg et al., 2009). During bundle displacement, force is applied to the mechanotransduction apparatus by tension in tip links (Pickles et al., 1984; Hackney and Furness, 2013) extending from the top of each stereocilium to the side wall of its taller neighbor, which modulates the open probability of the mechano-electrical transducer (MT) channels. Because the channels detect at most a few hundred nanometers of motion at the tops of the stereocilia, transduction is endowed with multiple phases of adaptation to ensure that the MT channels are poised at their maximum sensitivity (Eatock, 2000; Fettiplace and Kim, 2014). The prevailing view has been that all phases of adaptation are regulated by a change in intracellular Ca^{2+} after influx of the ion via the Ca^{2+}-selective MT channels. However, there has been recent dispute about this mechanism in mammalian hair cells and whether, as in nonmammals, Ca^{2+} entry is required (Peng et al., 2013; Corns et al., 2014). The two groups reached different conclusions about the effects of altering Ca^{2+} influx or changing the concentration or buffering of intracellular Ca^{2+}. In one case (Peng et al., 2013), these manipulations had little effect on adaptation, whereas in the other (Corns et al., 2014), all modulated adaptation.

Although the molecular identity of the MT channel is still uncertain, recent studies have suggested that transmembrane channel–like protein isoform 1 (TMC1) and isoform 2 (TMC2) are possible pore-forming subunits of the channel (Kawashima et al., 2011; Kim and Fettiplace, 2013; Pan et al., 2013). The *Beethoven* ($Tmc1^{Bth}$) mutant is a mouse model for progressive hearing loss (DFNA36) caused by a point mutation producing a methionine to lysine substitution at position 412 of TMC1 (Vreugde et al., 2002), which may be located in the ion conduction pathway (Pan et al., 2013), and might therefore influence channel properties. We have characterized the MT channel in the *Beethoven* mutant, confirming that, as with the *Tmc1* mutant, it has an altered selectivity for Ca^{2+} (Kim and Fettiplace, 2013; Pan et al., 2013), and we then exploited this feature to investigate the role of Ca^{2+} in MT channel adaptation. These results, taken together with those derived from other manipulations of Ca^{2+} influx and its cytoplasmic concentration, are consistent with a major component of adaptation being mediated by a change in intracellular Ca^{2+}.

The Journal of General Physiology

MATERIALS AND METHODS

Mouse mutants

Beethoven (*Tmc1^Bth/Bth*) mice were obtained from K. Steel (King's College, London, England, UK) and W. Marcotti (Sheffield University, Sheffield, England, UK). *Tmc1^Bth/Bth* encodes a point mutation at residue 412, predicted to cause a methionine to lysine substitution (Vreugde et al., 2002). *Tmc2* mutant mice (B6.129S5-*Tmc2^tm1Lex*/Mmucd) were obtained from the Mutant Mouse Regional Resource Center (University of California, Davis, Davis, CA) and were used to generate double mutants *Tmc1^Bth/Bth*:*Tmc2^−/−*. Mice were genotyped from tail clips taken after dissection for the electrophysiology recordings or immunolabeling (Marcotti et al., 2006; Kim et al., 2013). In both cases, the experimenter was blind to the genotype. Mice, postnatal days (P) 3–9 were killed by decapitation, as specified by the Institutional Animal Care and Use Committees of the University of Wisconsin-Madison according to current National Institutes of Health guidelines. The cochlea was removed, and the organ of Corti was dissected in a solution composed of (mM): 150 NaCl, 6 KCl, 1.5 CaCl$_2$, 2 Na-pyruvate, 8 D-glucose, and 10 Na-HEPES, pH 7.4 (osmolarity of 315 mOsm). Either apical or basal coils of the excised organ of Corti were fixed in a microscope chamber under strands of dental floss and viewed through a long working-distance 63× water-immersion objective on a microscope (DMLFS; Leica). The effect of endolymph-like Ca^{2+} (0.04 mM) (Bosher and Warren, 1978; Ikeda et al., 1987) on transduction was studied by local application from a nearby puffer pipette containing (mM): 150 NaCl, 0.04 CaCl$_2$ (buffered with 4 HEDTA), 2 Na-pyruvate, 8 D-glucose, and 10 Na-HEPES, pH 7.4. For each extracellular solution, the fluid jet for bundle stimulation was filled with the same solution.

Electrophysiology and hair bundle stimulation

MT currents were recorded from outer hair cells (OHCs) and inner hair cells (IHCs) at room temperature (21–23°C) as described previously (Beurg et al., 2006, 2014). Patch electrodes were filled with an intracellular solution of composition (mM): 130 CsCl, 3 MgATP, 10 Tris phosphocreatine, 1 EGTA (1 BAPTA for the two-pulse adaptation experiment), 0.5 GTP, 0.5 cyclic AMP, and 10 Cs-HEPES, pH 7.2 (∼295 mOsm/l). They were connected to an amplifier (Axopatch 200B; Molecular Devices) with a 5-kHz output filter. Membrane potentials were corrected for a liquid junction potential of −4 mV. Single MT channel currents were isolated by brief treatment with extracellular saline containing 5 mM BAPTA to sever the majority of the tip links (Beurg et al., 2006; Kim et al., 2013).

MT currents were elicited as described previously (Kim and Fettiplace, 2013; Corns et al., 2014) using a fluid jet in which saline is ejected or withdrawn through the 10-μm tip of a glass pipette, with the flow generated by flexure in a piezoelectric disk. The flow, and hence the force applied to the hair bundle, is proportional to the driving voltage across the piezoelectric disk. The amplitude and time course of hair bundle motion during fluid jet stimulation were quantified by projecting an image of the OHC bundle onto a pair of photodiodes (LD 2–5; Centronics) at 240× (Crawford and Fettiplace, 1985; Kim and Fettiplace, 2013; Fig. S1). Because of the difficulty of the procedure, which requires optimal orientation of the preparation to produce a bright bundle, the bundle displacement was not calibrated in every experiment. The fluid jet was preferred to a rigid probe (Beurg et al., 2006; Peng et al., 2013) because it does not require any prior contact with the hair bundle, which could affect its resting position, and is also likely to evoke a more uniform stereociliary displacement (Corns et al., 2014); however, it suffers from the drawback that stimulus onsets are filtered, and therefore slower, and so adaptation kinetics could not be determined accurately. The relationship between

MT current, I, and bundle displacement, ΔX, was fitted with a single Boltzmann equation: $I/I_{MAX} = 1/(1 + \exp(-(\Delta X - X_{0.5})/X_S))$, where I_{MAX} = maximum current, $X_{0.5}$ = bundle displacement for half-maximum current, and X_S = slope factor expressing width of relation.

Calcium selectivity

The calcium selectivity of the MT channel was determined as described previously (Beurg et al., 2006; Kim and Fettiplace, 2013) by measuring the Ca^{2+} reversal potential (V$_{rev}$) using a CsCl-based intracellular solution containing (mM) 135 CsCl, 3 MgATP, 10 Tris phosphocreatine, 1 EGTA-CsOH, and 10 HEPES, pH 7.2 (osmolarity of 293 mOsm/l), and a high Ca^{2+} extracellular solution containing (mM) 100 CaCl$_2$, 20 N-methylglucamine, 6 Tris, and 10 D-glucose, pH 7.4, which was applied as described above and also included in the fluid jet. Reversal potentials were corrected for the liquid junction potential of −9 mV. The relative permeability, P$_{Ca}$/P$_{Cs}$, was calculated from the Goldman–Hodgkin–Katz equation:

$$P_{Ca}/P_{Cs} = \left\{ a_1 \left[Cs^+ \right]_o \big/ 4 \right\} \times \left\{ \exp(\theta) \right\} \times$$
$$\left\{ 1 + \exp(\theta) \right\} \big/ \left\{ a_2 \left[Ca^{2+} \right]_o - a_3 \left[Ca^{2+} \right]_i \left(\exp (2\theta) \right) \right\}, \quad (1)$$

where $\theta = (V_{rev}F/RT)$; RT/F has its usual meaning with a value at room temperature of 25.6 mV; [Cs$^+$] is the intracellular Cs$^+$ concentration (140 mM); [Ca^{2+}]$_o$ is the extracellular Ca^{2+} concentration (100 mM); [Ca^{2+}]$_i$ is the intracellular Ca^{2+} concentration (0, 1, or 2.5 mM); and a1, a2, and a3 are the activity coefficients for Cs$^+$ (Partanen, 2010) and Ca^{2+} (Rard and Clegg, 1997) with values of a1 = 0.73 for intracellular Cs$^+$, a2 = 0.52 for 100 mM extracellular Ca^{2+}, and a3 = 0.89 or 0.84 for 1 or 2.5 mM of intracellular Ca^{2+}, respectively. For those internal solutions containing elevated Ca^{2+}, MgATP was reduced to 0.1 mM to minimize Ca^{2+} buffering by ATP.

Immunostaining

Immunofluorescence labeling for PMCA2, the plasma membrane CaATPase pump, was performed as described previously (Chen et al., 2012), using an affinity-purified rabbit polyclonal antibody (NR2; Thermo Fisher Scientific). P5–P10 mice were decapitated, and cochleas were fixed in 4% paraformaldehyde in phosphate buffer for 40 min at room temperature. Isolated cochlear coils were treated with 0.5% Triton X-100, immersed for 1 h in 10% goat serum (Invitrogen) to block nonspecific labeling, and incubated overnight at 4°C with primary NR2 antibody. Specimens were labeled with Alexa Fluor 488 goat anti–rabbit IgG secondary antibody followed by Alexa Fluor 568 phalloidin (Invitrogen), which defines the hair bundle by its actin labeling. Mounted tissue was viewed under a 60× (NA = 1.4; ELWD Planfluor; Nikon) oil-immersion objective in a laser scanning confocal microscope (A1; Nikon). Four cochleas were characterized from *Tmc1^+/+* and four from *Tmc1^Bth/Bth* mice. In each, the fluorescence intensities were quantified by averaging over areas of interest drawn around the hair bundle (Chen et al., 2012) in confocal images taken under identical conditions and photomultiplier settings using ImageJ (Fiji) software (National Institutes of Health). Fluorescence intensities were measured for 50 OHC bundles chosen at random in each preparation.

Statistical analysis

Unless otherwise stated, all values are quoted as means ± SD. Statistical comparisons of means were made by Student's two-tailed *t* test.

Online supplemental material

Fig. S1 shows calibration of the fluid jet–evoked hair bundle motion during a two-pulse adaptation experiment by imaging the bundle on

a dual photodiode. The online supplemental material is available at http://www.jgp.org/cgi/content/full/jgp.201511458/DC1.

RESULTS

MT channels and Ca²⁺ selectivity in *Beethoven* mutant mice

MT currents from OHCs of wild-type ($Tmc1^{+/+}$) and littermate mutant ($Tmc1^{Bth/Bth}$) *Beethoven* mice were recorded during hair bundle displacements with a piezoelectric fluid jet (Kros et al., 1992; Kim and Fettiplace, 2013). The maximum amplitude of the MT current was similar at least up to postnatal day (P) 9 in all genotypes tested, indicating that, unlike *dn* mutation in *Tmc1* (Kim and Fettiplace,

2013), the *Beethoven* mutation does not impair mechanotransduction in apical OHCs. Because early on the bundles have a normal shape, a corollary is that the single–MT channel conductance was unaffected by the *Beethoven* mutation (Fig. 1, A–E). Although, as observed previously, there was an increase in OHC MT channel conductance from apex to base (Beurg et al., 2014, 2015), the conductance at neither location was reduced relative to wild type in $Tmc1^{Bth/Bth}$. The basal values are most diagnostic, because they show a marked twofold reduction in the $Tmc1^{-/-}$ (Beurg et al., 2014), but here there was no significant difference between the wild-type and *Beethoven* mutant. There was also no effect of the *Beethoven* mutation on the MT channel conductance in IHCs (Fig. 1 E).
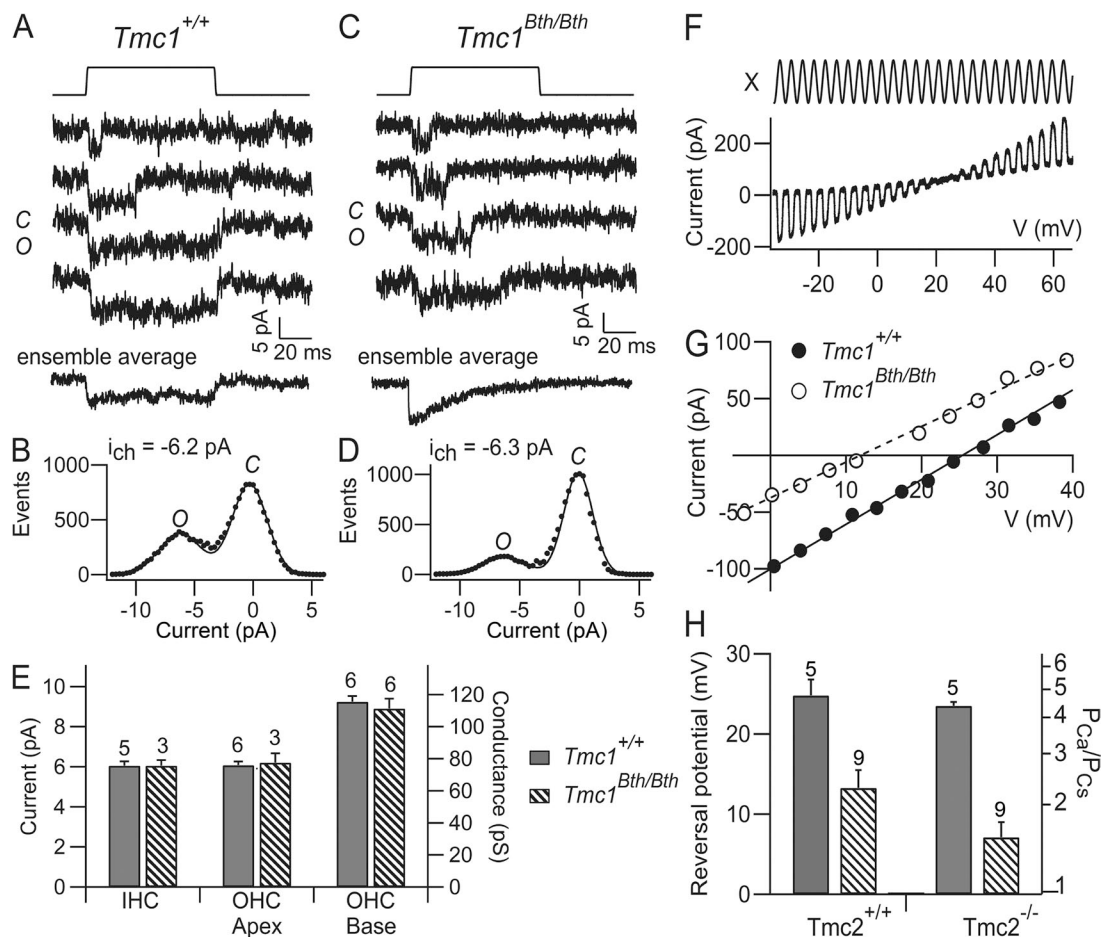
Figure 1. MT channel conductance and Ca²⁺ selectivity in $Tmc1^{Bth/Bth}$ mice. (A) Four examples of single MT channel currents, recorded in a P5 apical IHC of $Tmc1^{+/+}$ mice in response to 0.1-µm step displacements of the hair bundle; below is the ensemble average of 14 presentations. (B) Amplitude histogram showing single-channel current of 6.2 pA. (C) Four examples of single MT channel currents recorded in a P5 apical IHC of $Tmc1^{Bth/Bth}$ mice in response to 0.1-µm step displacements of the hair bundle; below is the ensemble average of 12 presentations. (D) Amplitude histogram showing single-channel current of 6.3 pA; both B and D were at a −84-mV holding potential in 1.5 mM of external Ca²⁺. (E) Bar plot showing collected single-channel currents in IHCs, apical OHCs, and basal OHCs for $Tmc1^{+/+}$ and $Tmc1^{Bth/Bth}$. Number of cells tested is shown above the columns. (F) Protocol for determining Ca²⁺ selectivity: mechanical hair bundle stimulus (top) evoking MT current (bottom) during voltage ramp from −40 to 70 mV. (G) Examples of MT current–voltage relationships recorded in apical OHCs from $Tmc1^{+/+}$ and $Tmc1^{Bth/Bth}$ mice in the voltage region around reversal potential. (H) Collected reversal potentials (left ordinate) and P_{Ca}/P_{Cs} (right ordinate) for $Tmc1^{+/+}$ and $Tmc1^{Bth/Bth}$ in $Tmc2^{+/+}$ and $Tmc2^{-/-}$ backgrounds. Numbers of OHCs tested are shown above the columns. Apical OHCs: P4–P6 mice. Error bars represent means ± SD.

Another manifestation of the properties of the MT channel pore is the ionic permeability, in particular its selectivity for Ca^{2+} over other cations. The Ca^{2+} selectivity of the MT channel in *Beethoven* was assayed by measuring the reversal potential of the transducer current under ionic conditions in which Ca^{2+} and Cs^+ were the only permeant cations in the extracellular and intracellular solutions, respectively (Beurg et al., 2006; Kim and Fettiplace, 2013). This enabled the permeability ratio, P_{Ca}/P_{Cs}, to be calculated (see Materials and methods). The reversal potential and relative Ca^{2+} permeability in

apical OHCs were both significantly reduced ($P < 0.001$) in *Tmc1^Bth/Bth^* mice compared with *Tmc1^+/+^* (Fig. 1, F–H). In the first postnatal week, there are concerns about the presence of TMC2, which is down-regulated at about P6 (Kawashima et al., 2011), and the knockout of which reduces the channel Ca^{2+} selectivity (Kim and Fettiplace, 2013). Although the Ca^{2+} selectivity in wild-type OHC MT channels decreases slightly with age up to P10 (Kim and Fettiplace, 2013), to exclude any contribution from TMC2 in the present experiments, double mutant mice (*Tmc1^Bth/Bth^:Tmc2^−/−^*), in which TMC2 was also not present,
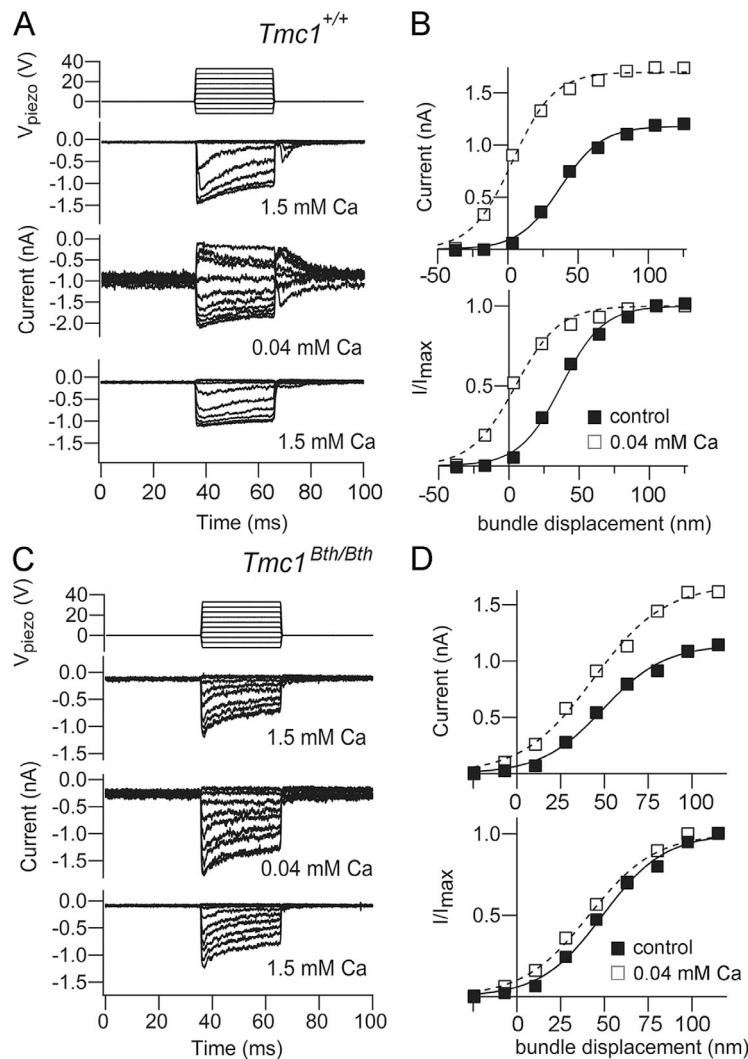
Figure 2. Effects of low endolymph-like Ca^{2+} on MT current in OHCs of *Tmc1^Bth/Bth^*. (A) MT currents recorded from a P5 OHC of *Tmc1^+/+^* mouse at -84 mV when the bundle was bathed in saline with 1.5 mM, 0.04 mM, and return control 1.5 mM of extracellular Ca^{2+}. Note that in 0.04 mM Ca^{2+}, the resting open probability increased in *Tmc1^+/+^*. (B) Current–displacement relations in *Tmc1^+/+^*, peak, I (top), and normalized (I/I_{max}; bottom) MT currents recorded from the OHC as a function of bundle displacement. (C) MT currents in P5 OHCs of *Tmc1^Bth/Bth^* mice at -84 mV when the bundle was bathed in saline with 1.5 mM, 0.04 mM, and return control 1.5 mM of extracellular Ca^{2+}. (D) Current–displacement relations in *Tmc1^Bth/Bth^* and maximum and normalized MT currents recorded from an OHC as a function of bundle displacement. The plots demonstrate a leftward shift of the MT current–displacement relation in *Tmc1^+/+^* (B) but not in *Tmc1^Bth/Bth^* mice (D). Sets of points fitted with Eq. 1 with the following parameters: B, $I_{MAX} = 1.2$ nA, $X_{0.5} = 38$ nm, $X_S = 15$ nm, and 1.5 mM Ca^{2+}; $I_{MAX} = 1.7$ nA, $X_{0.5} = 5$ nm, $X_S = 15$ nm, and 0.04 mM Ca^{2+}. D, $I_{MAX} = 1.14$ nA, $X_{0.5} = 46$ nm, $X_S = 16$ nm, and 1.5 mM Ca^{2+}; $I_{MAX} = 1.68$ nA, $X_{0.5} = 41$ nm, $X_S = 19$ nm, and 0.04 mM Ca^{2+}. In both genotypes, the maximum current was increased in 0.04 mM Ca^{2+} relative to 1.5 mM Ca^{2+}. In B and D, hair bundle displacement was calculated from the piezoelectric driving voltage (V_{piezo}) using the calibrations described in Results.

were also examined and a similar reduction in Ca^{2+} selectivity was observed (Fig. 1 H). In both the presence and absence of TMC2, there was a half to two thirds reduction in the Ca^{2+} selectivity of the OHC MT channel in $Tmc1^{Bth/Bth}$ relative to wild type; a comparable reduction in Ca^{2+} selectivity was reported for IHCs of $Tmc1^{Bth/-}$ relative to wild type (Pan et al., 2013).

Ca^{2+}-dependent adaptation of the MT current in OHCs of *Beethoven* mice

Through its action on transducer channel adaptation, Ca^{2+} modulates the fraction of the transducer current activated at the bundle's resting position (i.e., the position in the absence of stimulation). Increasing Ca^{2+} influx through the MT channels decreases channel open probability and thus promotes adaptation, whereas reducing Ca^{2+} influx, by lowering its extracellular concentration or depolarizing the cell to near the Ca^{2+} equilibrium potential, increases the channel open probability (Corey and Hudspeth, 1983; Assad et al., 1989; Crawford et al., 1991; Ricci et al., 1998). The effect of Ca^{2+} on adaptation of the MT current in *Beethoven* mutants was tested

by comparing experiments in which bundles were bathed in saline containing 1.5 mM Ca^{2+} as in perilymph, and low extracellular Ca^{2+}, 0.04 mM, similar to endolymph to which they are exposed in vivo (Bosher and Warren, 1978; Ikeda et al., 1987). In OHCs from $Tmc1^{+/+}$ mice, reducing the extracellular Ca^{2+} concentration from 1.5 to 0.04 mM at −84 mV increased MT channel resting P_{open} (Fig. 2, A and B) from (mean ± SD) 0.02 ± 0.01 ($n = 8$) to 0.43 ± 0.02 ($n = 5$), as reported previously (Johnson et al., 2011). However, in OHCs of $Tmc1^{Bth/Bth}$ mice, there was a smaller increase in the MT channel resting P_{open} (Fig. 2, C and D), from 0.03 ± 0.01 ($n = 6$; 1.5 mM Ca^{2+}) to 0.19 ± 0.07 ($n = 5$; 0.04 mM Ca^{2+}). The values for P_{open} in the low Ca^{2+} were significantly different between genotypes (P < 0.001).

Apart from regulating adaptation, Ca^{2+} is also known to block inward current through the MT channels from the external surface, with a half-blocking concentration of ∼1 mM (Ricci and Fettiplace, 1998; Kim et al., 2013); therefore, lowering extracellular Ca^{2+} to its concentration in endolymph increases the current by relieving Ca^{2+} block of the channel (Corey and Hudspeth, 1983;
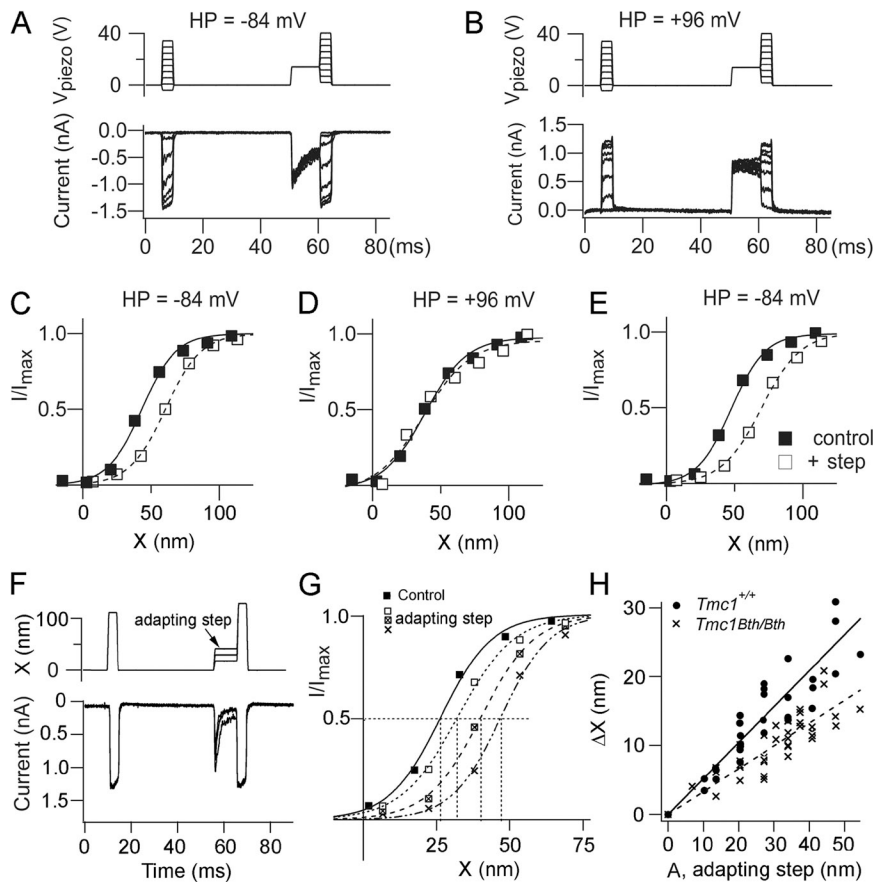
Figure 3. Adaptive shift in a paired-pulse protocol is reduced in OHCs of $Tmc1^{Bth/Bth}$. (A and B) Superimposed MT currents recorded from a P4 OHC in response to paired-pulse hair bundle stimulation, with the second pulse preceded by a 10-ms adapting step. Holding potential (HP) was −84 mV (A) and +96 mV (B). (C–E) Current–displacement relationships for first pulse (S1; closed squares) and second pulse (S2; open squares) at −84, +96, and return to −84 mV. Change in holding potential produced by a 100-ms depolarizing step starting 8 ms before the mechanical stimuli. MT currents, I, scaled to maximum current, I_{MAX}; displacements were determined from piezoelectric driver voltage (V_{piezo}) by calibration as described in Results. Note that the adaptive shift in the current–displacement relationship at −84 mV was abolished at +96 mV. Each set of points fit with Eq. 1 with the following parameters: C, $I_{MAX} = 1.4$ nA, $X_{0.5} = 42$ nm, and $X_S = 12$ nm, S1; $I_{MAX} = 1.38$ nA, $X_{0.5} = 60$ nm, and $X_S = 12$ nm, S2; D, $I_{MAX} = 1.2$ nA, $X_{0.5} = 40$ nm, and $X_S = 18$ nm, S1; $I_{MAX} = 1.2$ nA, $X_{0.5} = 39$ nm, and $X_S = 15$ nm, S2; E, $I_{MAX} = 1.4$ nA, $X_{0.5} = 48$ nm, and $X_S = 12$ nm, S1; $I_{MAX} = 1.39$ nA, $X_{0.5} = 70$ nm, and $X_S = 15$ nm, S2. Recordings from apical P4 OHCs of $Tmc1^{+/+}$; similar results were seen in six OHCs of P4–P6 mice. (F) Paired-pulse experiment in which the amplitude of the adapting step (A) was varied, shown for one test pulse. (G) For each adapting step, a family of test pulses was presented to determine the current–displacement relationships, shown for control (closed squares) and three adapting steps. For each adapting step, the current–displacement relationship was fitted with a single Boltzmann to determine ΔX, the shift in half-amplitude. (H) The shift, ΔX, is plotted against (A), the size of the adapting step for five OHCs of $Tmc1^{+/+}$ (closed circles) and five OHCs of $Tmc1^{Bth/Bth}$ (crosses). All points are for each genotype fitted with a straight line: slope, 0.52 ± 0.02 in $Tmc1^{+/+}$ and 0.33 ± 0.01 in $Tmc1^{Bth/Bth}$; apical OHCs of P4–P6 mice.

Ricci and Fettiplace, 1998; Fettiplace and Kim, 2014). In the present experiments, reducing extracellular Ca^{2+} concentration from 1.5 to 0.04 mM increased I_{max}, the peak MT current amplitude: I_{max} (0.04/1.5) = 1.44 ± 0.17 ($n = 5$) in $Tmc1^{+/+}$, and I_{max} (0.04/1.5) = 1.45 ± 0.05 ($n = 5$) in $Tmc1^{Bth/Bth}$ mice, with no significant difference in I_{max} (0.04/1.5) values between genotypes. This indicates that the site of Ca^{2+} blockade within the channel is unaffected by the point mutation in $Tmc1^{Bth/Bth}$.

To confirm whether OHCs from $Tmc1^{Bth/Bth}$ mice possess reduced adaptation, a paired-pulse protocol was used in which two series of brief mechanical test steps (4 ms) were delivered to the hair bundle, one before and the other during a nonsaturating adapting step (10 ms). This paired-pulse protocol was applied to OHCs held at −84 (Fig. 3 A) and +96 mV (Fig. 3 B). The displacement of the hair bundle evoked by a given fluid jet stimulus was in some experiments calibrated by imaging the hair bundle on a photodiode pair (Crawford and Fettiplace, 1985; Fig. S1). Because the procedure requires optimal orientation of the preparation to produce a bright bundle, the bundle displacement was not calibrated in every experiment. In those cells where it was, the fluid jet calibration, expressed as nanometers of OHC bundle displacement per volt of piezoelectric driving voltage, was 3.6 ± 0.4 nm/V ($n = 16$) in $Tmc1^{+/+}$ and 3.2 ± 0.5 nm/V ($n = 10$) in $Tmc^{Bth/Bth}$. The two means are not significantly different, implying that there is no major change in OHC bundle stiffness in the Beethoven

mutant. The calibrations were used to derive the relationship between MT current and displacement. After the adapting step at a −84-mV holding potential, the relationship was shifted to the right along the displacement axis compared with that preceding the adapting step (Fig. 3 C), but at +96 mV, the adaptive shift was absent (Fig. 3 D); retesting after the holding potential was returned to −84 mV showed that the adaptive shift returned (Fig. 3 E). The existence of an adaptive shift, present at −84 mV and absent at +96 mV, was seen in all cells studied whether the bundle displacement was measured directly in the experiment (Fig. S1) or was inferred from piezoelectric driving voltage, V_{piezo}, using calibration values given above (Fig. 3, C–E). Furthermore, the same voltage-dependent behavior of adaptation was observed in the OHCs of $Tmc1^{Bth/Bth}$ as well as of $Tmc1^{+/+}$ mice. The adaptive shift in the current–displacement relationship is usually thought to result from a change in intracellular Ca^{2+} after influx of the ion through the MT channels; such influx will be small or absent on depolarizing to large positive potentials (here, +96 mV) that approach the Ca^{2+} equilibrium potential (Assad et al., 1989; Crawford et al., 1991).

To examine the efficacy of adaptation, the same two-pulse protocol was used, but the size of the adapting step was varied (Fig. 3, F–H). For each size of adapting step (A), the shift in the current–displacement relationship (ΔX) was determined and plotted against A (Fig. 3 H). The linear fit to these plots in five OHCs gave a slope
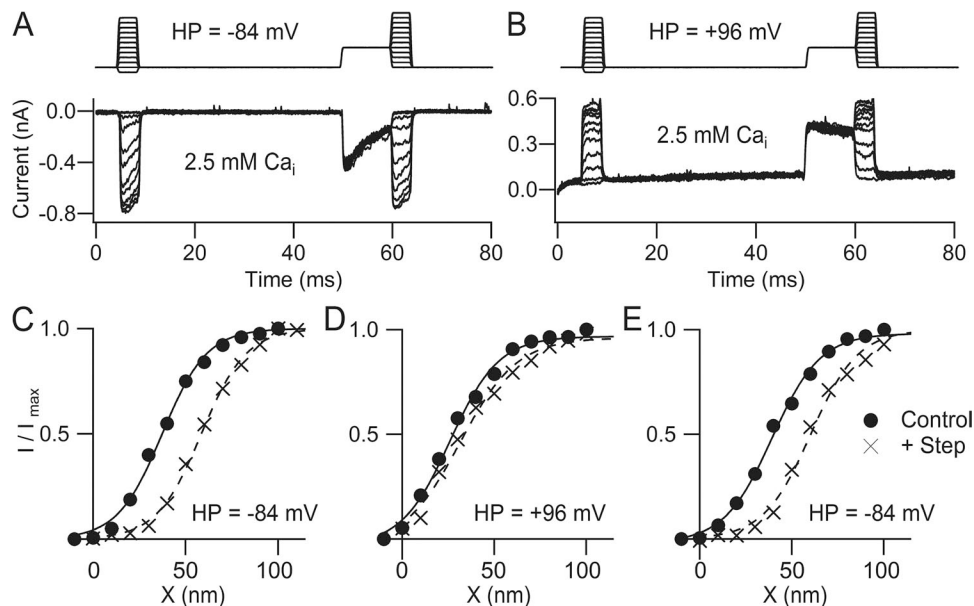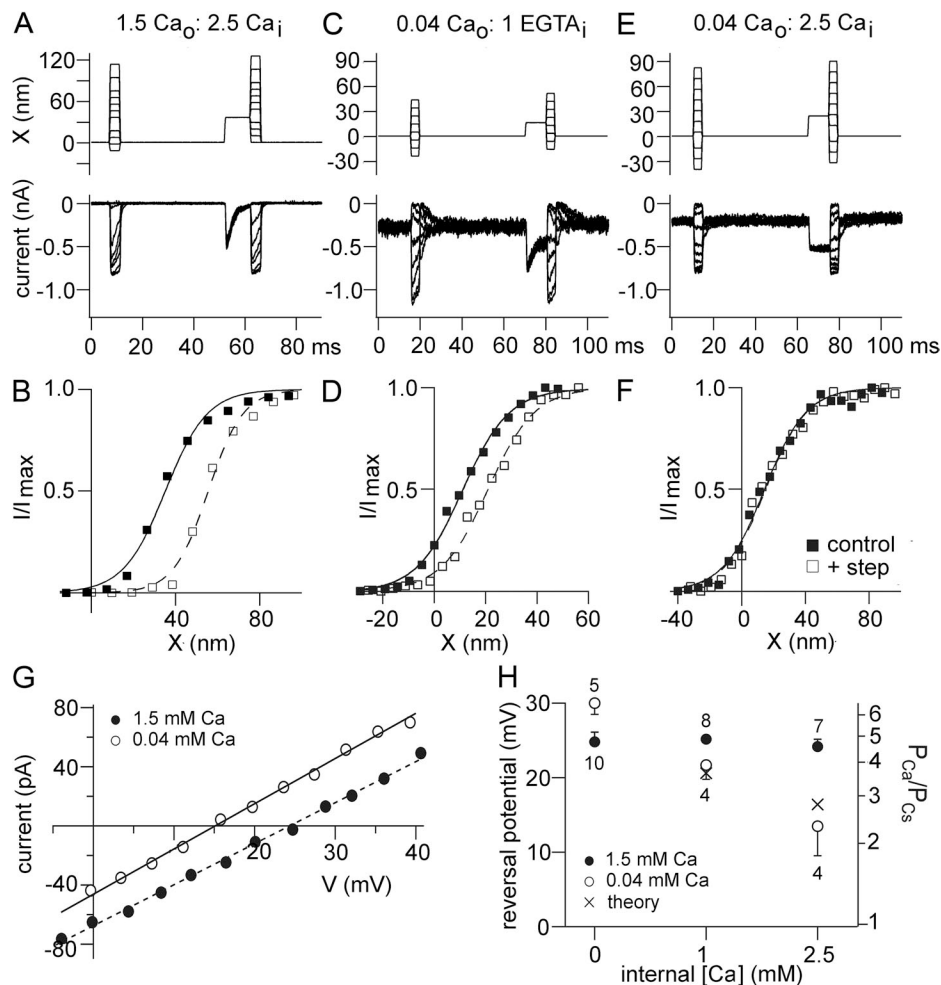

Figure 4. Adaptive shift in a paired-pulse protocol in 2.5 mM of intracellular Ca^{2+}. (A and B) Superimposed MT currents recorded from a P4 OHC in response to paired-pulse hair bundle stimulation, with the second pulse preceded by an adapting step as in Fig. 3. Holding potential (HP) was −84 (A) and +96 mV (B). (C–E) Current–displacement relationships for first pulse (S1; closed circles) and second pulse (S2; crosses) recorded at −84, +96, and return to −84 mV. MT currents, I, scaled to maximum current I_{MAX}; displacements were determined from piezoelectric driver voltage (V_{piezo}) by calibration as described in Results. Note that the adaptive shift in the current–displacement relationship persisted at −84 mV, even though the recording pipette contained 2.5 mM Ca^{2+}, and this shift was abolished at +96 mV. Sets of points fit with the Boltzmann equation (see Materials and methods).

that was significantly (P < 0.02) smaller in $Tmc1^{Bth/Bth}$ (0.33 ± 0.01; n = 5) than in $Tmc1^{+/+}$ mice (0.52 ± 0.02, n = 5; mean ± SD). It might be argued that such a difference reflects different hair bundle mechanics between wild type and mutant, but this is unlikely because the slope ($\Delta X/A$) is dimensionless (ΔX and A are measured in the same units), and furthermore, there was no difference in fluid jet sensitivity between OHC hair bundles of $Tmc1^{+/+}$ and $Tmc1^{Bth/Bth}$ (see above). The results demonstrate that OHCs in the *Beethoven* mutant still retain adaptation but at a reduced level.

Intracellular Ca^{2+} at the channel

The results so far are most easily explained by postulating that impairment of MT adaptation in *Beethoven* is attributable to a smaller Ca^{2+} influx through MT channels with reduced Ca^{2+} permeability. Doubt has previously been cast on the role of cytoplasmic Ca^{2+} in regulating adaptation because, among other observations, adaptation was unaffected by raising intracellular Ca^{2+} to a level that might be expected to exceed that normally present during adaptation (Peng et al., 2013). We confirmed this result, obtaining a slope factor ($\Delta X/A$) of 0.52 ± 0.03 (n = 11), but then found that the adaptation observed with a patch-pipette solution containing 2.5 mM Ca^{2+} was in all OHCs significantly reduced or abolished (P < 0.001) on depolarizing to +96 mV (Fig. 4): at +96 mV, the slope factor ($\Delta X/A$) was 0.17 ± 0.10 (n = 11; range of 0.002 – 0.310). This result suggests that a major component of transducer adaptation is mediated by

Figure 5. Adaptive shift in different extracellular and cytoplasmic Ca^{2+} concentrations. (A) Superimposed MT currents in paired-pulse protocol for 1.5 mM of external Ca^{2+} (Ca$_O$) and 2.5 mM of internal Ca^{2+} (Ca$_i$). (B) Current–displacement relations for first pulse (control; closed squares) and second pulse (+step; open squares) of records in A. (C) Superimposed MT currents in paired-pulse protocol for 0.04 mM Ca$_O$ and 0 Ca$_i$ buffered with 1 mM EGTA. (D) Current–displacement relations for first pulse (closed squares) and second pulse (open squares) for records in C. (E) Superimposed MT currents in paired-pulse protocol for 0.04 mM Ca$_O$ and 2.5 mM Ca$_i$. (F) Current–displacement relations for first pulse (closed squares) and second pulse (open squares) for records in E. Note that there were adaptive shifts in B and D, but not in F. (G) Current–voltage relationships of MT channel as in Fig. 1 G, with 1.5 mM Ca$_O$ and 2.5 mM Ca$_i$ (closed circles) and 0.04 mM Ca$_O$ and 2.5 mM Ca$_i$ (open circles). (H) Reversal potentials and permeability ratios, P$_{Ca}$/P$_{Cs}$, with initial exposure to Ca$_o$ = 1.5 mM (closed circles) and prolonged prior exposure to Ca$_o$ = 0.04 mM (open circles) as a function of intracellular Ca^{2+} concentration, Ca$_i$. Error bars represent the mean ± SD, with the number of experiments given above the points. Theoretical values are calculated from Eq. 1, assuming Ca$_i$ = 0 mM (crosses). All recordings were in apical OHCs of P4–P5 mice.

Ca^{2+} entry, but it does not rule out that an additional process independent of Ca^{2+} influx can make some contribution (Peng et al., 2013).

A possible explanation for the lack of effect of high intracellular Ca^{2+} introduced via the patch pipette solution is that there is significant accumulation of Ca^{2+} at the inner face of the channel when it is open, but Ca^{2+} influx is still much reduced on depolarizing toward the Ca^{2+} equilibrium potential. Such a hypothesis is consistent with two other observations in which the two-pulse adaptive shifts in the current displacement relation were documented under different combinations of intracellular and extracellular Ca^{2+} (Fig. 5). First, if the hair bundle was bathed in saline containing an endolymph-like, 0.04-mM Ca^{2+}, an adaptive shift in the current–displacement relation still occurred when recording with an intracellular solution buffered with 1 mM EGTA (Fig. 5, C and D). In low extracellular Ca^{2+}, the efficacy of adaptation, expressed as $\Delta X/A$, was 0.49 ± 0.11 (mean ± SD; $n = 5$). However, the shift was much reduced on recording with 2.5 mM of intracellular Ca^{2+} (Fig. 5, E and F), with a $\Delta X/A$ value of 0.11 ± 0.14 ($n = 7$), not significantly different from 0 (P = 0.08). Evidence that the high, 2.5 mM of intracellular Ca^{2+} reached the channel was that it produced partial block of the MT current: the mean amplitude of the current was 1.44 ± 0.15 nA when recording with submicromolar intracellular Ca^{2+} buffered with 1 mM EGTA, and was reduced to 0.61 ± 0.21 nA with 2.5 mM of intracellular Ca^{2+}.

If, during recording with 2.5 mM of intracellular Ca^{2+}, a comparably high concentration is achieved at the internal face of the MT channel, it should theoretically reduce the reversal potential of the MT current determined as described above (see Materials and methods). The reversal potential was measured while bathing the hair bundle in 100 mM of extracellular Ca^{2+}, and was not significantly altered when either 1 or 2.5 mM Ca^{2+} was in the recording pipette solution (Fig. 5 H). The expected reduction in reversal potential, V$_{rev}$, was estimated from the constant field equation, Eq. 1 (see Materials and methods), assuming a constant permeability ratio P$_{Ca}$/P$_{Cs}$; for 2.5 mM of intracellular Ca^{2+}, the predicted decrease in reversal potential compared with zero intracellular Ca^{2+} was roughly 10 mV.

An explanation for this discrepancy is that when the preparation is immersed in 1.5 mM Ca^{2+}-perilymph, there is stereociliary accumulation of the divalent cation before and during performing the measurement with 100 mM. To address this possibility, before determining the reversal potential, the hair bundle was bathed in 0.04 mM Ca^{2+} for 5 or more minutes to lower bundle Ca^{2+}. With this added manipulation, a significant change in reversal potential was seen experimentally, similar to that predicted by Eq. 1 (Fig. 5, G and H). An important conclusion is that the stereociliary Ca^{2+} is substantially elevated when the bundles are bathed in

perilymph. A corollary is that the reversal potential, and hence the permeability ratio P$_{Ca}$/P$_{Cs}$, is underestimated in such conditions. Even when the internal solution was buffered with 1 mM EGTA or BAPTA, the reversal potential was increased to 30.0 ± 1.5 mV ($n = 5$) after exposure to 0.04 mM Ca^{2+} saline (Fig. 5 H). Using this value for reversal potential and assuming zero intracellular Ca^{2+}, a permeability ratio P$_{Ca}$/P$_{Cs}$ of 6.7 ± 0.2 was calculated.
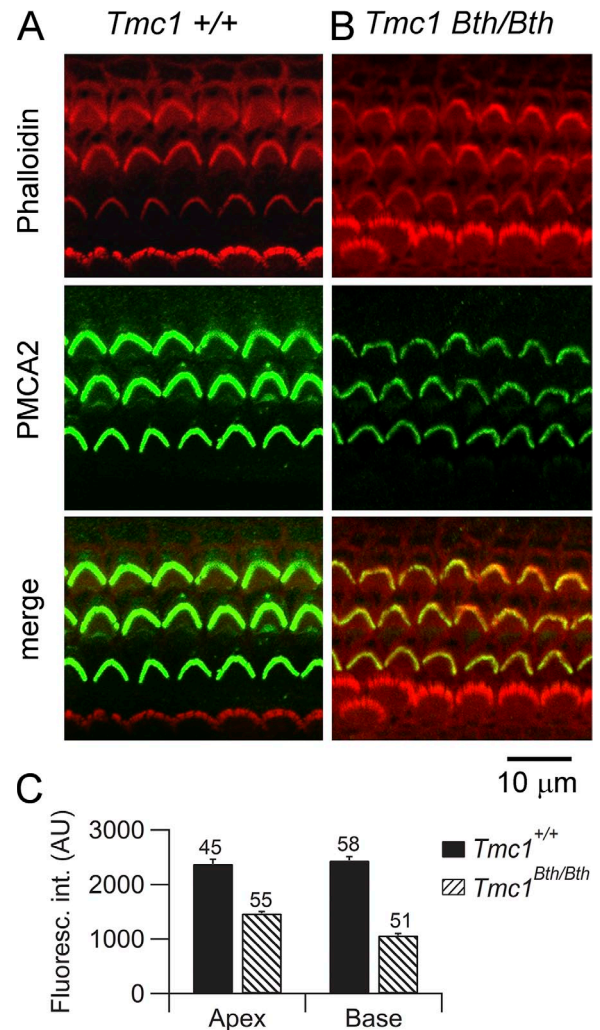
Figure 6. Hair bundle expression of PMCA2 Ca^{2+} pump is reduced in *Beethoven* mice. (A) Immunofluorescent labeling of the apical coil cochlea from a *Tmc1*$^{+/+}$ P6 mouse. (Top) Phalloidin-labeled hair bundles of three rows of OHCs above and one row of IHCs below. (Middle) PMCA2 labeling in which OHC bundles label more than IHCs. (Bottom) A merged image. (B) Immunofluorescent labeling of an apical cochlear coil from a *Tmc1*$^{Bth/Bth}$ P6 mouse. (Top) Phalloidin-labeled hair bundles of three rows of OHCs above and one row of IHCs below. (Middle) PMCA2 labeling in which OHC bundles label more than IHCs. (Bottom) A merged image. Label in *Tmc1*$^{Bth/Bth}$ is much less pronounced than that in *Tmc1*$^{+/+}$ mice. (C) Collected measurements of OHC bundle intensity in *Tmc1*$^{+/+}$ (closed bar) and *Tmc1*$^{Bth/Bth}$ (hatched bar) for apical and basal OHCs. Numbers of cells measured are shown above the bars from three P6–P8 mice in each genotype. Error bars represent means ± SD.

With this permeability ratio, and a reversal potential of 24.6 mV obtained with exposure to 1.5 mM Ca^{2+} saline (Fig. 5 H), the intracellular Ca^{2+} is estimated to be in at least 3 mM. The equivalent measurement performed on the *Beethoven* mutant after prior exposure to 0.04 mM Ca^{2+} saline gave a reversal potential $\sim$2 mV more positive than that obtained under conditions where the preparation was first exposed to normal 1.5 mM Ca^{2+} saline. The reversal potential after low Ca^{2+} exposure was 11.2 ± 1.9 mV (n = 7), from which a P_{Ca}/P_{Cs} of 1.9 ± 0.2 was calculated, compared with the P_{Ca}/P_{Cs} value of 1.5 ± 0.2 in 1.5 mM Ca^{2+} saline, with both measurements being made on a $Tmc2^{-/-}$ background.

Immunostaining for the plasma membrane CaATPase pump

Ca^{2+} ions entering OHC stereocilia via the MT channels bind to calcium-buffering proteins, such as oncomodulin (Hackney et al., 2005), and are extruded via the PMCA2a isoform of the plasma membrane CaATPase pump (Dumont et al., 2001; Beurg et al., 2010), which is present at high density on the OHC stereociliary membrane. As reported previously (Chen et al., 2012), PMCA2 labeling is greater in bundles of OHCs than in IHCs; however, there are additional pumps in the IHC lateral membrane, probably conferred by the PMCA1 isoform, to cope with Ca^{2+} influx via the voltage-dependent Ca^{2+} channels in IHCs (Dumont et al., 2001; Chen et al., 2012). Changes in OHC expression of the PMCA2 with developmental age and cochlear location closely follow the functional appearance of the MT current (Chen et al., 2012). Because the *Beethoven* mutation causes a reduction in the Ca^{2+} selectivity of the MT channel, we hypothesized that the pump density would be affected in the mutant. Immunofluorescent labeling for PMCA2 confirmed it was strongly expressed in hair bundles of OHCs (Fig. 6, A and B). In $Tmc1^{Bth/Bth}$, PMCA2 expression was reduced in both apical and basal OHCs (Fig. 6 C), with the mean reduction being 40% at the apex and 58% at the base, and the differences with respect to the control both being significant (P < 0.001).

DISCUSSION

MT channels in *Beethoven*

The molecular identity of the MT channel is still unclear, but recent work has identified two molecules (LHFPL5 and TMIE) implicated in mechanotransduction (Xiong et al., 2012; Zhao et al., 2014) that interact with protocadherin-15 at the lower end of the tip link (Kazmierczak et al., 2007). However, each of these deafness-associated membrane proteins is small and unlikely to be a pore-forming subunit of the channel (Xiong et al., 2012; Zhao et al., 2014; Beurg et al., 2015). In contrast, TMC1 and TMC2 are larger and could be pore-forming subunits of the MT channel (Kawashima et al., 2011; Pan et al., 2013). Here, we have examined the effects of a point mutation in TMC1, *Beethoven*, which is potentially in the ion conduction pathway (Pan et al., 2013) and so might influence MT channel properties. The primary outcome of the *Beethoven* mutation on MT channel function was an approximate halving in P_{Ca}/P_{Cs}, the relative Ca^{2+} selectivity of the channel (Fig. 1 H). However, we found no effect on the single MT channel conductance in either apical or basal OHCs or in IHCs, or on the block of the channel by extracellular Ca^{2+}. Both findings disagree with an earlier report focused on IHCs (Pan et al., 2013), which claimed a change in the single-channel conductance in a *Beethoven* mutant. The lack of effect of the *Beethoven* point mutation on either MT channel conductance or on blockade by external Ca^{2+} weakens the conclusion that the M412K point mutation resides in the pore region of the MT channel, a line of argument used to maintain that TMC1 is a component of the pore (Pan et al., 2013). This type of behavior contrasts with localization of the pore in the mechano-sensitive channel protein Piezo by a single glutamate substitution (E2133A in piezo1 and E2416 in piezo2) to halve channel conductance (Coste et al., 2015). The $Tmc1^{Bth/Bth}$ mutation resembles $Tmc2^{-/-}$ in causing a change in the Ca^{2+} selectivity with no alteration in unitary conductance (Kim and Fettiplace, 2013; Kim et al., 2013). Our results do not exclude TMC1 as a pore component but merely suggest that the *Beethoven* mutation is unlikely to reside in the pore region.

Ca^{2+}-dependent adaptation

A secondary consequence of the *Beethoven* mutation was an $\sim$40% reduction in the sensitivity of OHC adaptation ($\Delta X/A$; Fig. 3 H). This consequence would be consistent with a halving in the Ca^{2+} influx through the channel, provided the Ca^{2+}-binding site for regulating adaptation was on the cytoplasmic side of the channel. In addition, there were smaller shifts in the current–displacement relationship for reduced extracellular Ca^{2+} (Fig. 2) in the mutant. In those experiments, the resting position of the current–displacement relationship, reflected in the control resting P_{open} of the channel, was normal, but either manipulation drew a reduced response. This implies that, besides the component of adaptation dependent on Ca^{2+} influx, some other adaptive mechanism must exist (Eatock, 2000; Peng et al., 2013) and be resistant to the *Beethoven* mutation or to elevating cytoplasmic Ca^{2+}. Such a mechanism might be mediated by tension in the tip link, adjusting its upper attachment point or the force it delivers to the MT channel. Nevertheless, because the adaptive shift revealed in paired-pulse experiments was largely eliminated on depolarization to near the Ca^{2+} equilibrium potential (Fig. 3), one component of MT

channel adaptation is likely to be regulated by a change in intracellular Ca^{2+}.

Three lines of evidence attest to the role of intracellular Ca^{2+} in regulating adaptation. The suppressive effects of depolarization and increased Ca^{2+} buffering have been contested (Peng et al., 2013; Corns et al., 2014), but both are indirect. The finding that adaptation is preserved when recording with a pipette solution containing 1.5 mM Ca^{2+} (Peng et al., 2013) seems definitive in arguing against a role for intracellular Ca^{2+}. We reproduced this observation with 2.5 mM of internal Ca^{2+} but then discovered that the adaptation was still suppressed by depolarization, and furthermore, if measurements were made when bathing the hair bundle in saline containing endolymph-like Ca^{2+} (40 µM), then adaptation was now abolished with the same 2.5 mM of internal Ca^{2+} (Fig. 5). The simplest explanation for this result is that there is accumulation of Ca^{2+} at the cytoplasmic face of the MT channel, reaching a concentration of several millimolar in external saline (1.5 mM Ca^{2+}). It should be noted that the internal concentration of Ca^{2+} can be higher than the external because of the additional effect on the driving force of a -80-mV holding potential that can theoretically produce a 500-fold concentration of the divalent ion.

Functional consequences of the *Beethoven* mutation

The origin of the progressive hearing loss phenotype in the *Beethoven* mutant mice (Vreugde et al., 2002; Marcotti et al., 2006) is unknown. One possibility from the results here is that the decreased Ca^{2+} permeability of the OHC MT channel is the main causative factor. Related to the reduced Ca^{2+} influx through the MT channels in *Beethoven* mutants, there was a smaller shift in the MT current–displacement relation in endolymphatic Ca^{2+} concentration, causing a smaller fraction of the current to be activated at the resting position of bundles bathed in low Ca^{2+} endolymph. The large resting open probability generates an inward current that normally depolarizes OHCs (Johnson et al., 2011), and as a consequence, its reduction in *Beethoven* mutants will hyperpolarize these cells. This hyperpolarization will shift the membrane potential negative to that optimal for prestin activation (about -50 mV), thereby decreasing cochlear sensitivity attributable to OHC amplification (Ashmore, 2008; Johnson et al., 2011). This does not account for the abnormality and depletion of IHCs, which precedes that of OHCs (Vreugde et al., 2002). However, the overall consequence is likely to be an increase in the compound action potential threshold despite the presence of functional MT channels.

The *Beethoven* mutation also results in a reduction in the stereociliary density of the PMCA2 pump responsible for extruding Ca^{2+} ions that have entered via the MT channels. The reduced expression of the pump may reflect homeostatic regulation in the face of a decreased Ca^{2+} influx through MT channels with half their normal permeability to that ion. Because several types of deafness have been attributed to defects in PMCA2 expression or pumping capacity in OHCs (Street et al., 1998; Bortolozzi et al., 2010), it is conceivable that this is an additional factor in the progressive deafness in *Beethoven*. However, if the decreased expression of PMCA2 results from a smaller influx and cytoplasmic concentration of Ca^{2+}, then it is possible that other genes are down-regulated in *Beethoven*, and these contribute to the deafness phenotype.

REFERENCES

Ashmore, J. 2008. Cochlear outer hair cell motility. *Physiol. Rev.* 88:173–210. http://dx.doi.org/10.1152/physrev.00044.2006

Assad, J.A., N. Hacohen, and D.P. Corey. 1989. Voltage dependence of adaptation and active bundle movement in bullfrog saccular hair cells. *Proc. Natl. Acad. Sci. USA.* 86:2918–2922. http://dx.doi.org/10.1073/pnas.86.8.2918

Beurg, M., M.G. Evans, C.M. Hackney, and R. Fettiplace. 2006. A large-conductance calcium-selective mechanotransducer channel in mammalian cochlear hair cells. *J. Neurosci.* 26:10992–11000. http://dx.doi.org/10.1523/JNEUROSCI.2188-06.2006

Beurg, M., R. Fettiplace, J.H. Nam, and A.J. Ricci. 2009. Localization of inner hair cell mechanotransducer channels using high-speed calcium imaging. *Nat. Neurosci.* 12:553–558. http://dx.doi.org/10.1038/nn.2295

Beurg, M., J.H. Nam, Q. Chen, and R. Fettiplace. 2010. Calcium balance and mechanotransduction in rat cochlear hair cells. *J. Neurophysiol.* 104:18–34. http://dx.doi.org/10.1152/jn.00019.2010

Beurg, M., K.X. Kim, and R. Fettiplace. 2014. Conductance and block of hair-cell mechanotransducer channels in transmembrane channel-like protein mutants. *J. Gen. Physiol.* 144:55–69. http://dx.doi.org/10.1085/jgp.201411173

Beurg, M., W. Xiong, B. Zhao, U. Müller, and R. Fettiplace. 2015. Subunit determination of the conductance of hair-cell mechanotransducer channels. *Proc. Natl. Acad. Sci. USA.* 112:1589–1594. http://dx.doi.org/10.1073/pnas.1420906112

Bortolozzi, M., M. Brini, N. Parkinson, G. Crispino, P. Scimemi, R.D. De Siati, F. Di Leva, A. Parker, S. Ortolano, E. Arslan, et al. 2010. The novel PMCA2 pump mutation Tommy impairs cytosolic calcium clearance in hair cells and links to deafness in mice. *J. Biol. Chem.* 285:37693–37703. http://dx.doi.org/10.1074/jbc.M110.170092

Bosher, S.K., and R.L. Warren. 1978. Very low calcium content of cochlear endolymph, an extracellular fluid. *Nature.* 273:377–378. http://dx.doi.org/10.1038/273377a0

Chen, Q., S. Mahendrasingam, J.A. Tickle, C.M. Hackney, D.N. Furness, and R. Fettiplace. 2012. The development, distribution and density of the plasma membrane calcium ATPase 2 calcium

pump in rat cochlear hair cells. *Eur. J. Neurosci.* 36:2302–2310. http://dx.doi.org/10.1111/j.1460-9568.2012.08159.x

Corey, D.P., and A.J. Hudspeth. 1983. Kinetics of the receptor current in bullfrog saccular hair cells. *J. Neurosci.* 3:962–976.

Corns, L.F., S.L. Johnson, C.J. Kros, and W. Marcotti. 2014. Calcium entry into stereocilia drives adaptation of the mechanoelectrical transducer current of mammalian cochlear hair cells. *Proc. Natl. Acad. Sci. USA.* 111:14918–14923. http://dx.doi.org/10.1073/pnas.1409920111

Coste, B., S.E. Murthy, J. Mathur, M. Schmidt, Y. Mechioukhi, P. Delmas, and A. Patapoutian. 2015. Piezo1 ion channel pore properties are dictated by C-terminal region. *Nat. Commun.* 6:7223. http://dx.doi.org/10.1038/ncomms8223

Crawford, A.C., and R. Fettiplace. 1985. The mechanical properties of ciliary bundles of turtle cochlear hair cells. *J. Physiol.* 364:359–379. http://dx.doi.org/10.1113/jphysiol.1985.sp015750

Crawford, A.C., M.G. Evans, and R. Fettiplace. 1991. The actions of calcium on the mechano-electrical transducer current of turtle hair cells. *J. Physiol.* 434:369–398. http://dx.doi.org/10.1113/jphysiol.1991.sp018475

Dumont, R.A., U. Lins, A.G. Filoteo, J.T. Penniston, B. Kachar, and P.G. Gillespie. 2001. Plasma membrane Ca^{2+}-ATPase isoform 2a is the PMCA of hair bundles. *J. Neurosci.* 21:5066–5078.

Eatock, R.A. 2000. Adaptation in hair cells. *Annu. Rev. Neurosci.* 23:285–314. http://dx.doi.org/10.1146/annurev.neuro.23.1.285

Fettiplace, R., and K.X. Kim. 2014. The physiology of mechanoelectrical transduction channels in hearing. *Physiol. Rev.* 94:951–986. http://dx.doi.org/10.1152/physrev.00038.2013

Hackney, C.M., and D.N. Furness. 2013. The composition and role of cross links in mechanoelectrical transduction in vertebrate sensory hair cells. *J. Cell Sci.* 126:1721–1731. http://dx.doi.org/10.1242/jcs.106120

Hackney, C.M., S. Mahendrasingam, A. Penn, and R. Fettiplace. 2005. The concentrations of calcium buffering proteins in mammalian cochlear hair cells. *J. Neurosci.* 25:7867–7875. http://dx.doi.org/10.1523/JNEUROSCI.1196-05.2005

Ikeda, K., J. Kusakari, T. Takasaka, and Y. Saito. 1987. The Ca^{2+} activity of cochlear endolymph of the guinea pig and the effect of inhibitors. *Hear. Res.* 26:117–125. http://dx.doi.org/10.1016/0378-5955(87)90040-2

Johnson, S.L., M. Beurg, W. Marcotti, and R. Fettiplace. 2011. Prestin-driven cochlear amplification is not limited by the outer hair cell membrane time constant. *Neuron.* 70:1143–1154. http://dx.doi.org/10.1016/j.neuron.2011.04.024

Kawashima, Y., G.S. Géléoc, K. Kurima, V. Labay, A. Lelli, Y. Asai, T. Makishima, D.K. Wu, C.C. Della Santina, J.R. Holt, and A.J. Griffith. 2011. Mechanotransduction in mouse inner ear hair cells requires transmembrane channel-like genes. *J. Clin. Invest.* 121:4796–4809. http://dx.doi.org/10.1172/JCI60405

Kazmierczak, P., H. Sakaguchi, J. Tokita, E.M. Wilson-Kubalek, R.A. Milligan, U. Müller, and B. Kachar. 2007. Cadherin 23 and protocadherin 15 interact to form tip-link filaments in sensory hair cells. *Nature.* 449:87–91. http://dx.doi.org/10.1038/nature06091

Kim, K.X., and R. Fettiplace. 2013. Developmental changes in the cochlear hair cell mechanotransducer channel and their regulation by transmembrane channel–like proteins. *J. Gen. Physiol.* 141:141–148. http://dx.doi.org/10.1085/jgp.201210913

Kim, K.X., M. Beurg, C.M. Hackney, D.N. Furness, S. Mahendrasingam, and R. Fettiplace. 2013. The role of transmembrane channel–like proteins in the operation of hair cell mechanotransducer

channels. *J. Gen. Physiol.* 142:493–505. http://dx.doi.org/10.1085/jgp.201311068

Kros, C.J., A. Rüsch, and G.P. Richardson. 1992. Mechano-electrical transducer currents in hair cells of the cultured neonatal mouse cochlea. *Proc. Biol. Sci.* 249:185–193. http://dx.doi.org/10.1098/rspb.1992.0102

Marcotti, W., A. Erven, S.L. Johnson, K.P. Steel, and C.J. Kros. 2006. Tmc1 is necessary for normal functional maturation and survival of inner and outer hair cells in the mouse cochlea. *J. Physiol.* 574:677–698. http://dx.doi.org/10.1113/jphysiol.2005.095661

Pan, B., G.S. Géléoc, Y. Asai, G.C. Horwitz, K. Kurima, K. Ishikawa, Y. Kawashima, A.J. Griffith, and J.R. Holt. 2013. TMC1 and TMC2 are components of the mechanotransduction channel in hair cells of the mammalian inner ear. *Neuron.* 79:504–515. http://dx.doi.org/10.1016/j.neuron.2013.06.019

Partanen, J.I. 2010. Re-evaluation of the thermodynamic activity quantities in aqueous rubidium and cesium chloride solutions at 25°C. *J. Chem. Eng. Data.* 55:249–257. http://dx.doi.org/10.1021/je900320r

Peng, A.W., T. Effertz, and A.J. Ricci. 2013. Adaptation of mammalian auditory hair cell mechanotransduction is independent of calcium entry. *Neuron.* 80:960–972. http://dx.doi.org/10.1016/j.neuron.2013.08.025

Pickles, J.O., S.D. Comis, and M.P. Osborne. 1984. Cross-links between stereocilia in the guinea pig organ of Corti, and their possible relation to sensory transduction. *Hear. Res.* 15:103–112. http://dx.doi.org/10.1016/0378-5955(84)90041-8

Rard, J.A., and S.L. Clegg. 1997. Critical evaluation of the thermodynamic properties of aqueous calcium chloride. 1. Osmotic and activity coefficients of 0–10.77 mol·kg^{-1} aqueous calcium chloride solutions at 298.15 K and correlation with extended Pitzer ion-interaction models. *J. Chem. Eng. Data.* 42:819–849. http://dx.doi.org/10.1021/je9700582

Ricci, A.J., and R. Fettiplace. 1998. Calcium permeation of the turtle hair cell mechanotransducer channel and its relation to the composition of endolymph. *J. Physiol.* 506:159–173. http://dx.doi.org/10.1111/j.1469-7793.1998.159bx.x

Ricci, A.J., Y.C. Wu, and R. Fettiplace. 1998. The endogenous calcium buffer and the time course of transducer adaptation in auditory hair cells. *J. Neurosci.* 18:8261–8277.

Schwander, M., B. Kachar, and U. Müller. 2010. Review series: The cell biology of hearing. *J. Cell Biol.* 190:9–20. http://dx.doi.org/10.1083/jcb.201001138

Street, V.A., J.W. McKee-Johnson, R.C. Fonseca, B.L. Tempel, and K. Noben-Trauth. 1998. Mutations in a plasma membrane Ca^{2+}-ATPase gene cause deafness in deafwaddler mice. *Nat. Genet.* 19:390–394. http://dx.doi.org/10.1038/1284

Vreugde, S., A. Erven, C.J. Kros, W. Marcotti, H. Fuchs, K. Kurima, E.R. Wilcox, T.B. Friedman, A.J. Griffith, R. Balling, et al. 2002. Beethoven, a mouse model for dominant, progressive hearing loss DFNA36. *Nat. Genet.* 30:257–258. http://dx.doi.org/10.1038/ng848

Xiong, W., N. Grillet, H.M. Elledge, T.F. Wagner, B. Zhao, K.R. Johnson, P. Kazmierczak, and U. Müller. 2012. TMHS is an integral component of the mechanotransduction machinery of cochlear hair cells. *Cell.* 151:1283–1295. http://dx.doi.org/10.1016/j.cell.2012.10.041

Zhao, B., Z. Wu, N. Grillet, L. Yan, W. Xiong, S. Harkins-Perry, and U. Müller. 2014. TMIE is an essential component of the mechanotransduction machinery of cochlear hair cells. *Neuron.* 84:954–967. http://dx.doi.org/10.1016/j.neuron.2014.10.041